

Efficient and standardized interface energy calculations in hybrid heterostructures using fictitious atoms surface passivation

Sreejith PALLIKKARA CHANDRASEKHARAN, Sofia APERGI, Charles CORNET*,
Laurent PEDESSEAU*

Univ Rennes, INSA Rennes, CNRS, Institut FOTON - UMR 6082, F-35000 Rennes, France

*Corresponding Authors

Correspondence to Charles Cornet (charles.cornet@insa-rennes.fr) and Laurent Pedesseau (laurent.pedesseau@insa-rennes.fr)

Abstract

Heterostructures combining diverse physico-chemical properties are increasingly in demand for a wide range of applications in modern science and technology. However, despite their importance in materials science, accurately determining absolute interface energies remains a major challenge. This difficulty arises from periodic boundary conditions, high computational costs of plane-wave methods, multipolar interactions in heterostructures, the need for thick slabs for interface convergence, and reconstructed surfaces on both slab faces. Here, we introduce a standardized and computationally efficient fictitious H^* charge passivation method for the surface termination, designed to accurately determine absolute interface energies in heterogeneous materials associations. This approach effectively addresses issues associated with surface reconstructions while significantly reducing computational costs within the framework of density functional theory. To demonstrate its reliability, we calculate the absolute interface energies for various quasi-lattice-matched and lattice-mismatched abrupt III-V/Si interfaces using the H^* passivation technique and benchmark the results against those obtained using conventional reconstructed surface methods. We further explore the early stages of strained epitaxial GaAs on Si(001). Finally, we assess the fictitious H^* passivation method, showing its effectiveness in minimizing electric dipole errors, reducing computational costs, and thus decreasing greenhouse gas emissions from high-performance computing. Finally, the potential of the approach to compute interface energies across a broad spectrum of materials is emphasized.

As *H. Kroemer* emphasized in his Nobel lecture, a deep understanding of interfaces between dissimilar materials is crucial, as they play a pivotal role in determining device performances^{1,2}. Especially, the knowledge of interface energy, whose atomic structure is very hard to resolve experimentally, provides a fundamental framework for predicting interface configuration, its physical properties, and may help to clarify processes involved during heteroepitaxy. Notably, the chemical mismatch between substrate atoms and the deposited layer leads to the formation of a hybrid interface³. Evaluating the energetics of heterointerfaces offers valuable insights into thermodynamic stability⁴⁻⁷, interfacial bonding⁶⁻⁹, electronic properties¹⁰⁻¹⁷, strain relaxation processes^{11,18,19}, and defect generation²⁰, particularly in polar-on-nonpolar systems²¹⁻²³. Such insights are essential in optimizing growth conditions^{24,25}, reducing defects^{22,26}, and enhancing the quality and performance of heterostructure devices for the next-generation technologies²⁷⁻²⁹.

Numerous studies have investigated interface energetics using a variety of experimental techniques. These include direct methods such as scanning microscopes³⁰, photoelectron spectroscopy³¹, calorimetric measurements³², as well as indirect approaches like inverse Wulff-Kaischew constructions and relative energy assessments³³. Despite these significant advances, the precise determination of absolute interface energy values remains largely underexplored, mainly inherent to challenges associated with obtaining accurate measurements as well as realistic and accurate theoretical simulations.

Ab initio atomistic studies have significantly contributed to our understanding of the atomic arrangements at the heterointerfaces^{7,13-15,22,23,34-41}. Several methods have been developed to evaluate interface energies in heteroepitaxial systems, including relative energy method (also known as the "superlattice" method) and absolute energy method. The relative energy method yields only relative values of interface energies and requires a convergence study of the total energy as a function of the material thickness^{7,13,14,36-38}. In contrast, calculating the absolute interface energy offers fundamental insights that are essential for understanding the behavior and properties of interfaces^{5,22,23,39-41}. In this approach, a slab

including a bottom surface, bulk substrate, hybrid interface, bulk layer, and top surface is constructed. The interface energy is determined by systematically subtracting the surface and bulk energy contributions from the total energy. This approach thus necessitates the inclusion of a large vacuum region to establish a true zero-energy reference point, enabling meaningful absolute comparisons across different configurations. Moreover, this approach enables precise definition of the mechanical and electronic properties at the interface, offering crucial insights into the grown epilayers, including wetting behavior^{5,42}, and potentially the equilibrium crystal shapes⁴³. Our previous studies determined the absolute interface energies of various GaP/Si heterostructure configurations using complex surface reconstruction methods^{22,23}. In these studies, both the bottom and top surfaces were atomically reconstructed based on assumed configurations extracted from the literature reports. A major challenge in calculating absolute interface energy lies in constructing a supercell that accommodates various surface reconstructions, while simultaneously: i) minimizing electric dipole interactions between the supercell and its periodic images by introducing large vacuum region; ii) achieving convergence of the absolute interface energy by incorporating a substantial amount of material on both sides of the interface; and iii) exploiting symmetry as much as possible to reduce computational cost.

In this paper, we introduce a robust and versatile fictitious H^{*} charge passivation method for the calculation of absolute interface energies, applicable to various heteroepitaxial systems. This method significantly enhances slab symmetry and substantially reduces computational costs. Furthermore, it effectively addresses challenges inherent to reconstructed surfaces in density functional theory (DFT) calculations^{44,45} including dipoles interactions errors originating from both the top and bottom surfaces of the heterostructure, as well as from the interface itself. In previous works, a fictitious H^{*} passivation strategy has been applied to investigate electronic properties of nanoparticles⁴⁶, absolute surface energies of various materials^{23,47}, and interface properties including electronic structure, charge density, mechanical/optical properties, and adhesion energies^{34,48-50}. Furthermore, previous studies often overlook the effects of electric dipoles caused by insufficient vacuum spacing

and the critical role of chemical potential. Although some DFT codes incorporate dipole-dipole corrections to partially address multipole interactions, these corrections are not sufficient and sometimes inadequate. Our work reveals that the H^* passivation-based interface energy calculations proposed here provide a robust and accurate means for determining the absolute interface energies of various heterostructures, including lattice-matched (GaP/Si) or strained ones (GaAs/Si). Finally, we demonstrate how the H^* passivation approach sweeps away errors resulting from electric dipole effects at the hetero-interface. This is achieved through non-stoichiometric abrupt interface calculations, analyzing interface structures across various thicknesses, and comparing charge densities of reconstructed and H^* passivated surfaces. In addition, we compare the computational expenses and environmental sustainability of both approaches.

Results

For an accurate computational determination of the absolute interface energy between two dissimilar materials, the influence of the top and bottom surfaces should be carefully cancelled. Assuming a given atomic reconstruction for these surfaces thus leads to specific dipoles or surface-stress-related effects, which can ultimately influence the accuracy of the calculated interface energy. The proposed H^* passivation approach, which replaces surface reconstruction atoms with fictitious atoms bonded directly to the bulk, offers three main advantages. First, surface passivation allows the top and bottom surfaces of the slab to mimic the bulk properties of a heterostructure. Second, the impact of multipoles disappears dramatically and naturally, a result that is beyond the capabilities of traditional DFT all-electron or plane-wave codes. Third, when combined with localized basis set codes such as SIESTA⁵¹⁻⁵³, this approach ensures convergence of the electric dipole and total energy for a polar slab, with negligible contributions from Coulombic interactions and surface dipoles arising from slab images⁵⁴. Recently, D. Bennett *et al.*⁵⁵ demonstrated that a localized basis offers superior scaling with system size and greater suitability to low-dimensional system, advantages that we exploit in this study.

Here, absolute interface energies for a Ga-abrupt GaP/Si(001) (quasi-lattice-matched) interface (where Si atoms are only bonded to Ga atoms at the interface) are compared using the H* passivation and the reconstructed surface approaches. The method is then applied to the bi-axially strained GaAs/Si(001) case and discussed with respect to the quantum-size effects of slab thickness on the non-converging behavior in interface energy calculations.

Absolute interface energy: reconstructed surfaces

The absolute interface energy of different III-V/Si systems was first calculated using stable, reconstructed top and bottom surface slabs. This approach enables the calculation of the absolute interface energy by eliminating the bulk and surface energy contributions from the total energy of the interface supercell slab per unit area (details in methods section). A thorough understanding of the predominant surface reconstructions of the two different materials in the heterostructure is crucial for this approach. The analysis of surface reconstructions must account for the system's polarity, the influence of electric dipoles on DFT calculations, and the associated computational costs. A comprehensive study of the absolute interface energies of III-V/Si heterostructures, based on free surfaces models, has been presented in our previous studies^{22,23}. In the present work, we employed a slab model, illustrated in Fig. 1a-d. Figure 1a shows a schematic of a supercell representing an abrupt GaP/Si(001) interface. This model includes stable reconstructed GaP(001)md(2x4) surface of the deposited material (Fig. b), and (Fig. c) the bottom reconstructed Si(001) surface. A Ga-abrupt interface was considered, with Ga atoms directly bonded to the silicon ones, as shown in Fig. 1d. To suppress electrostatic charge-charge and multipole interactions between the slab and its periodic images, a vacuum region of approximately 400 Å was introduced, following the approach detailed in the ref.²³, and further described in methods section.

Absolute interface energy: H* passivation on surfaces

The second modeling strategy proposed here is to use fictitious H* charge passivation method for surface modeling to overcome the challenges associated with limited knowledge of surface reconstructions across various heterostructures, the large system sizes needed to capture these effects, and the influence of electric dipole interactions. This H* passivation

approach effectively compensates for the dangling bonds at the surface, thereby mimicking the bulk-like electronic environment⁴⁶. Similarly, the interface energy is here defined as the excess or deficit of the total system energy relative to the sum of the energies of the top and bottom subsurface slabs and the bulk regions. The subsurface slabs incorporate energy contributions from H^* passivation, thereby simplifying computations by eliminating the need to separately account for the H^* energy. To model surface passivation, we employ fictitious H^* atoms with assigned net charge: 0.75e for fictitious atoms bonded to group V atoms, 1.25e for fictitious atoms bonded to group III atoms, and 1e for the ones bonded to Si atoms. In our previous works, we have validated the reliability of this methodology for calculating both polar and non-polar surface energies²³.

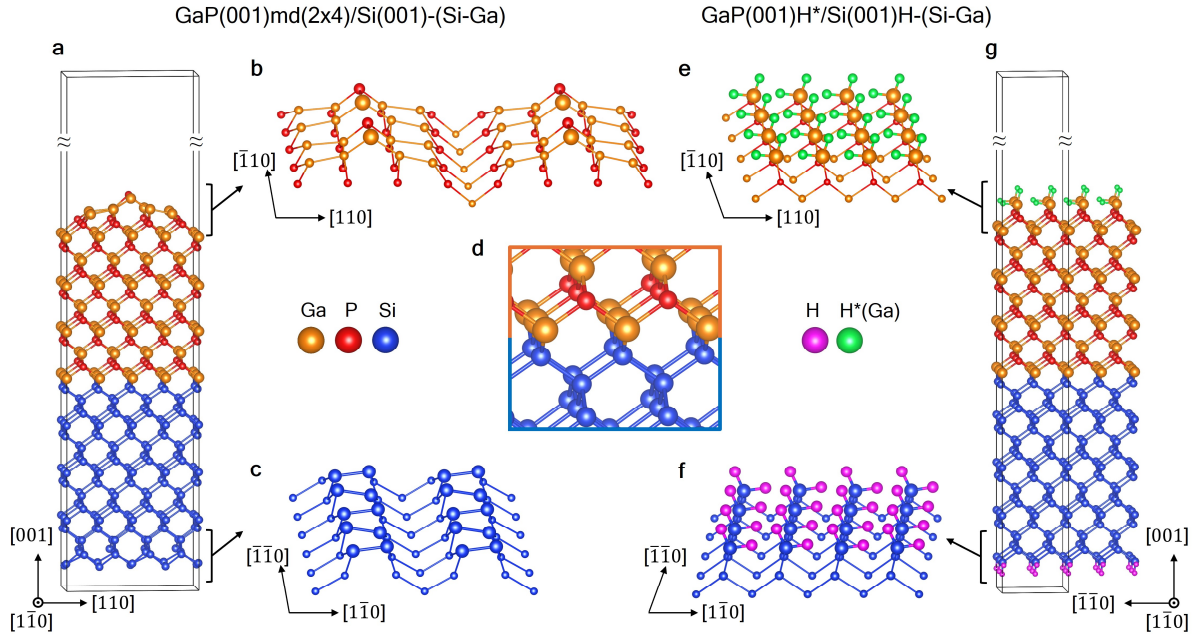


Fig. 1. Representation of relaxed slab models considered for determining absolute interface energies of GaP/Si. **a** Total slab model used for implementation of the reconstructed surface method, with **b** the reconstructed GaP(001)md(2x4) on top and **c** the Si(001) bottom surface for the **d** abrupt interface configuration. **e** top and **f** bottom view of H^* and H passivated surface terminations to compensate charges, and **g** the overall supercell model to determine absolute interface energy with the H^* passivation method.

In general, the absolute interface energy $I_{\gamma_{\text{Bottom}}^{\text{Top}}}$ for the interface I, where Top and Bottom represent the specific subsurface slabs of the material system is defined as:

$$I_{Y_{\text{Bottom}}^{\text{Top}}} = \frac{E_{\text{slab}}^{\text{int}} - \sum_{i=\text{Top,Bottom}} \left(\frac{1}{2} E_i^{\text{sub-surf}} \right) - \sum_j \left(N_j^{\text{bulk}} \mu_j^{\text{bulk}} \right) - \sum_{j,k} \left(\Delta N_j \mu_k \right)}{A} \quad (1)$$

where $E_{\text{slab}}^{\text{int}}$ is the total energy of the interface supercell slab, $E_i^{\text{sub-surf}}$ is the Top and Bottom subsurface slabs energies, μ_j^{bulk} is the chemical potential of the N_j^{bulk} atoms, and ΔN_j is the stoichiometry and μ_k is the chemical potential of the elements k of the composing material j . A is the in-plane surface area of the slabs.

Here, the analysis contains three distinct elements, with group-III and V atoms at the top and Si at the bottom of the heterostructure. As discussed in our previous work²³, the slab, subsurfaces, and interface each maintain distinct stoichiometries. The stoichiometry is quantified by $\Delta N_{\text{III-V}}$ for the III-V material and ΔN_{Si} for silicon.

From the above Eq. (1) the final expression for the absolute interface energy in the studied heterostructure is:

$$I_{Y_{\text{Si}}^{\text{III-V}}} = \frac{E_{\text{slab}}^{\text{int}} - \frac{1}{2} (E_{\text{III-V}}^{\text{sub-surf}}) - \frac{1}{2} (E_{\text{Si}}^{\text{sub-surf}}) - N_{\text{III-V}}^{\text{bulk}} \mu_{\text{III-V}}^{\text{bulk}} - N_{\text{Si}}^{\text{bulk}} \mu_{\text{Si}}^{\text{bulk}} - \Delta N_{\text{III-V}} \mu_V - \Delta N_{\text{Si}} \mu_{\text{Si}}}{A} \quad (2)$$

where $E_{\text{slab}}^{\text{int}}$ is the total energy of the interface supercell slab, $E_{\text{III-V}}^{\text{sub-surf}}$ and $E_{\text{Si}}^{\text{sub-surf}}$ are the total energies of III-V and Si subsurface slabs. The chemical potentials of bulk III-V and Si atoms are denoted as $\mu_{\text{III-V}}^{\text{bulk}}$ and $\mu_{\text{Si}}^{\text{bulk}}$, while $N_{\text{III-V}}^{\text{bulk}}$ and $N_{\text{Si}}^{\text{bulk}}$ are the corresponding number of bulk atoms. The stoichiometry of the III-V and Si material are given by $\Delta N_{\text{III-V}}$ and ΔN_{Si} with μ_V and μ_{Si} representing the chemical potentials of top (V) and bottom (Si) species, and A is the in-plane surface area of the slabs. The relationship simplifies naturally under the silicon surface condition ($\Delta N_{\text{Si}} = 0$). Interestingly, fictitious H^* energy is embedded in the subsurface term, eliminating the need for separate accounting. Similarly to the surface reconstruction method, that requires separate surface energy calculations, this approach needs a separate subsurface slab energy calculation.

The schematic representation of the relaxed slab considered for H^* passivation methodology is illustrated in Fig. 1d-g. As shown in Fig. 1d, similar Ga-abrupt interfaces are modeled, for both approaches studied. Here, the atoms of the top surface (Fig. 1e) are

passivated with $H^*(Ga)$ and a compensation charge of $1.25e$, while the atoms of the bottom Si surface (Fig. 1f) are passivated with H atoms to neutralize charges. The complete H^* passivated supercell used for absolute interface energy calculations is depicted in Fig. 1g. Notably, the supercell is reduced to half the size of that used in the reconstructed surface method (Fig. 1a), offering computational efficiency. Additionally, a vacuum thickness of approximately 400 \AA is introduced to eliminate spurious electrostatic charge-charge and dipole-dipole interactions between the slab and its image (details in methods section).

GaP/Si: quasi-lattice matched interface

Absolute interface energies with both reconstructed surfaces and H^* passivated surfaces approaches are computed within the thermodynamic limit for a quasi-lattice matched GaP/Si heterointerface. For GaP, we used the thermodynamic range determined by the heat formation energy of -0.928 eV^{23} , so that the interface energy is given between the two thermodynamic limits corresponding to the formation of bulk Ga and P respectively : the Ga-rich and P-rich limits. Here, we have used the previously reported Ga-abrupt absolute interface energies for two possible surface reconstructions of GaP in the (001) growth direction, specifically $GaP(001)(2 \times 4)$ and $GaP(001)md(2 \times 4)$. The calculated interface energies were evaluated as a function of phosphorus chemical potential variations ($\Delta\mu_P$) and the resulting trends are illustrated in Fig. 2a, with detailed values also listed in Table S1. From our previous results, the reconstructed surfaces method led to interface energies of 40.8 meV/\AA^2 (Ga-rich) and 72.0 meV/\AA^2 (P-rich) for $GaP(001)(2 \times 4)$, and 38.5 meV/\AA^2 (Ga-rich) and 69.7 meV/\AA^2 (P-rich) for $GaP(001)md(2 \times 4)$, respectively. On the other hand, using the H^* passivation approach, we obtained values of 43.6 meV/\AA^2 under Ga-rich conditions and 74.7 meV/\AA^2 under P-rich conditions. These results align well with those derived from the surface reconstruction method, having an error margin of less than 5 meV/\AA^2 (assigned to dipole interactions, as will be shown later).

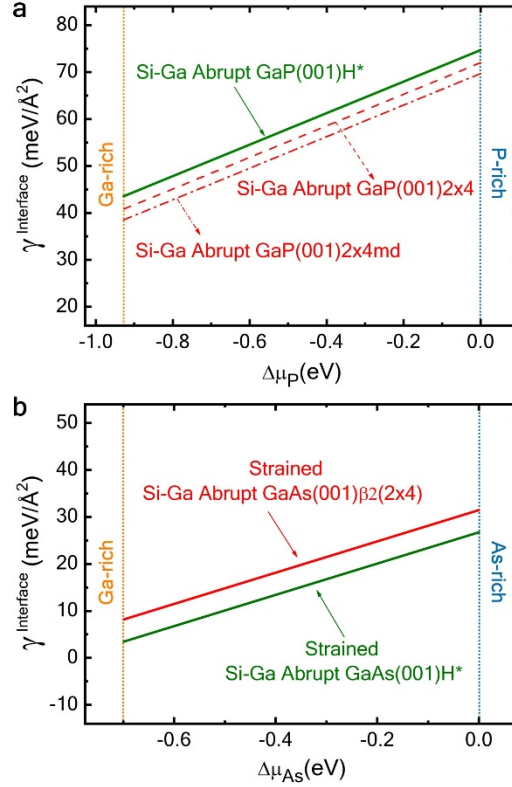


Fig. 2. Comparison of absolute interface energies ($\gamma^{\text{Interface}}$) calculation following the two different methods. a Absolute interface energies for GaP/Si with Ga-abrupt interfaces were calculated using the H* passivated method (green) and compared with previously reported GaP(001)(2x4) and GaP(001)md(2x4) surface reconstruction methods (red), as a function of the chemical potential of $\Delta\mu_P$. **b** Absolute interface energies for strained GaAs/Si with Ga-abrupt interfaces, calculated using the surface reconstruction method (red) and compared to the H* passivation approach (green), as a function of the chemical potential variations $\Delta\mu_{\text{As}}$.

GaAs/Si: lattice mismatched & strained growth

This study is now generalized to a lattice-mismatched heterointerface. In the following section, we examine the biaxially strained epitaxial integration of GaAs on Si using both methodologies. For GaAs, the surface and interface energies are governed by the variations of the chemical potentials of arsenic μ_{As} and gallium μ_{Ga} , which reflect the thermodynamic conditions under which each element can exist within the bulk or at the surface of the GaAs material. Indeed, these chemical potentials play a critical role in determining the stability and morphology of the heterointerface. In this work, the heat of formation of GaAs, $\Delta H_f(\text{GaAs})$, was determined to be -0.70 eV, consistent with previously reported values in the literature⁵⁶. A comprehensive description of the methodology is provided in the methods section. This

value delimits the thermodynamic stability window of GaAs, extending from Ga-rich to As-rich conditions, as illustrated in Fig. 2b.

In the early stages of epitaxial growth, before the plastic relaxation, GaAs grows pseudomorphically on the Si substrate, accommodating the lattice mismatch (experimentally measured $\approx 4\%$)^{57,58}. This results in a bi-axial compressive strain in the plane of the interface and in a corresponding elongation along the (001) growth direction. To accurately account for this strain, we considered both the bi-axially strained bulk and surface structures, as outlined in the Supplementary information (see details in Supplementary Fig. S2 and Supplementary note 1).

To determine the interface energies of a strained GaAs/Si heterostructure using a reconstructed approach, we analyzed the strained GaAs(001) $\beta 2(2 \times 4)$ surface on top, one of the stable GaAs surfaces in the (001) direction⁵⁶, and stable reconstructed Si(001)c(4x2) at the bottom⁴². Supplementary Fig. S3 illustrates the studied GaAs surfaces, with further details provided in Supplementary note 1. The methodology for determining absolute interface energies is comprehensively described in the methods section. A schematic representation of the reconstructed GaAs/Si interface is illustrated in Supplementary Fig. S4a-d. The interface energy varies from 8.2 meV/Å² (Ga-rich) to 31.5 meV/Å² (As-rich), within the thermodynamic range, as shown in Fig. 2b, and summarized in Supplementary Table S1.

Next, the strained interface energy is calculated using the fictitious H* passivation on the surfaces to ensure charge compensation and to mimic bulk-like properties on the surfaces, as previously demonstrated for the GaP/Si heterostructure. Supplementary Fig. S3 shows a schematic comparison of the strained GaAs surface slab structures for the GaAs/Si interface using surface-reconstructed and H* passivation methods, with the supercell size reduced to one-fourth. Additionally, Supplementary Fig. S4 further compares the GaAs/Si interface slabs for both approaches, incorporating an additional supercell size reduction by half. Using this approach, the calculated interface energies are 3.5 meV/Å² and 26.7 meV/Å² under extreme Ga-rich and As-rich thermodynamic conditions, respectively. Figure 2b compares the calculated interface energies from the H* passivation approach with those from

the reconstructed across the thermodynamic range, and Supplementary Table 1 summarizes the results. These results highlight the robustness of the H^* passivation method for determining absolute interface energies, achieving an accuracy within $5 \text{ meV}/\text{\AA}^2$. Importantly, the H^* -passivation approach requires a significantly smaller lateral supercell size compared to conventional calculations involving reconstructed surfaces. Compared to the GaP/Si interface, the GaAs/Si(001) heterostructure exhibits similar thermodynamic behavior, showing lower interface energies toward the Ga-rich side due to the similar Ga-abrupt configuration. Notably, under Ga-rich conditions, the bi-axially strained GaAs/Si interface energies are drastically lowered relative to GaP/Si. The observed trend in the interface energies for bi-axially strained heterostructures can be attributed to a combined effect of chemical inhomogeneity at the interface and structural distortions resulting from lattice misfit¹⁸. Recent calorimetric measurements by *Calvin et al.* even reported negative interface energies in the ZnS/InP heterostructure, which exhibits a pronounced lattice mismatch of approximately 8.4%³².

The evolution of the calculated interface energy with the GaAs thickness considered in the slab is then studied by computing different slabs having different thicknesses (Fig. 3a and Fig. 3b). Both approaches exhibit convergence in interface energy per atom ($N(\text{Ga}, \text{As})$) with increasing GaAs thickness under Ga-rich conditions (Fig. 3a), adjusted with solid lines as a guide to the eyes (see Supplementary note 2), where larger discrepancies between the two methods are observed at lower thickness likely due to surface dipole effects (discussed later in more details). Additionally, a linear divergence (not shown here) in interface energy values emerges with increasing GaAs slab thickness due to underestimated bulk energy contributions. To address this issue, we applied the Boettger correction^{59,60}. The resulting corrected interface energies are shown in Fig. 3a (inset), and exhibit no further evolution with the GaAs thickness, demonstrating the reliability of this correction even for large supercells and enabling accurate comparison between the two approaches. However, it is important to note that this correction does not account for surface dipole contributions. In contrast, the H^* passivation method effectively eliminates the influence of dipoles arising from surface

reconstructions, leading to a more accurate interface energy compared to the reconstructed surface method, as also shown in Fig. 3a (inset).

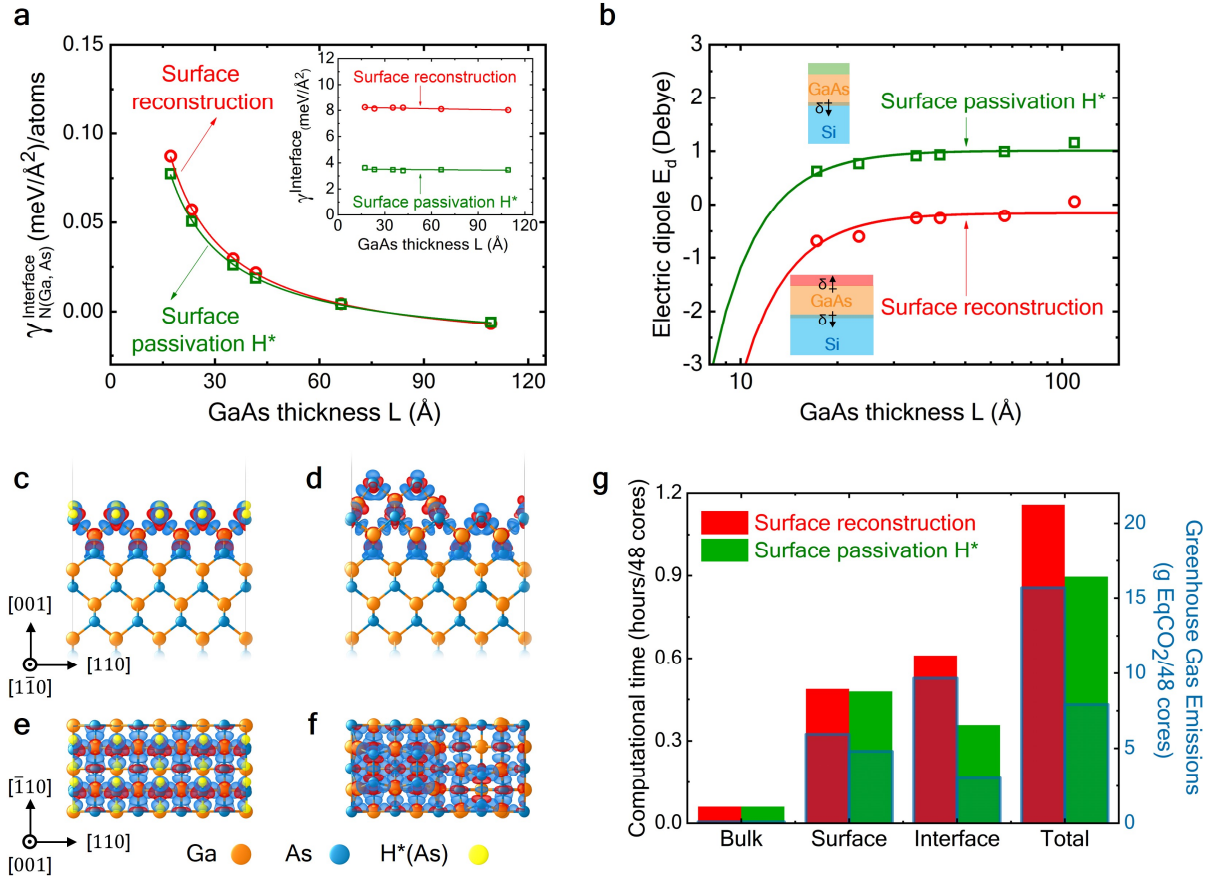


Fig. 3. Impact and advantages of H* passivation methods. **a** Bi-axially strained GaAs/Si(001) interface energy per atoms ($\gamma_{\text{N(Ga,As)}}^{\text{Interface}}$) with increasing GaAs thickness (L) under Ga-rich conditions (with solids lines as a guide-to-the-eye (see Supplementary note 2); corrected interface energies are shown in the inset). **b** Total electric dipole values as a function of material thickness (L) for both methods, fitted with solids lines (see Supplementary note 2), dipole directions are illustrated in the inset figures. Charge density distributions (at isosurface level = 0.03 e/Å³) showing the top and side views for the surface passivated H* (**c** and **e**) and surface reconstructed systems (**d** and **f**). **g** Comparison of the two methods in terms of computational time and greenhouse gas emissions.

Impact on electric dipole interactions

To further assess the potential of the H* passivation method, we analyzed the evolution of the total electric dipole $E_d(L)$ (in Debye) as a function of the GaAs thickness considered on the substrate, using both the reconstructed surface and H* passivation approaches, as shown in

Fig. 3b, with the vacuum thickness fixed at 400 Å. The solid lines are the best fit using the analytical expressions for dipole-dipole interactions⁶¹ for both curves. Details of the fitting parameters are provided in Supplementary note 2. Our previous studies demonstrated that at a vacuum spacing of at least 150 Å is necessary to minimize dipole interactions between periodic images, as evidenced by the highly polar GaP(111)A Ga-trimer surface slab²³. In the abrupt interface case chosen in this work, H* passivation captures only the dipoles at the interface (pointing downward from Ga to Si as illustrated in Fig. 3b) while eliminating surface charge interactions. In contrast, the surface reconstruction method includes a combined dipole contribution from both the reconstructed surface and the interface, reflecting misaligned and mixed charge interactions (as illustrated in Fig 3b). In the same Figure 3b, electric dipoles calculated using the H* passivated heterostructure are consistent with the analytical expression of dipole-dipole interactions (solid line), whereas the surface-reconstructed heterostructure exhibits deviations at lower GaAs thickness⁶¹. This discrepancy likely arises from additional dipole-dipole and multipole interactions, consistent with observations in other heterointerfaces^{62,63}. The possible multipole interactions (Supplementary Fig. S5) influencing the surface and interface decreases with increasing GaAs thickness. This analysis sheds light on the influence of induced dipole interactions on the surface and interface, and their impact on absolute interface energy calculations. In this case, in addition to axial dipoles, the reconstructed surface method exhibits parasitic dipole effects induced by surface stress. Moreover, reconstructed surface method shows in-plane inhomogeneity in the spatial distribution of charges related to the surface reconstruction. To explore this behavior, we examined the charge density distributions (at isosurface level = 0.03 e/Å³), in the top surface layers for both approaches, as presented in Figures 3c-f. In these figures, blue and red regions indicate positive and negative charge densities, respectively. The results indicate that the H* passivated heterostructure preserves bulk-like charge distribution at the surface (Fig. 3c, e), while the surface-reconstructed configuration exhibits pronounced disturbances and excess charge accumulation in the top layer (Fig. 3d, f), thus potentially impacting interface studies.

Impact on computational cost and greenhouse gas emissions

Finally, we assess the impact of our proposed method for calculating absolute interface energy on both computational time and greenhouse gas emissions, specifically CO₂ emissions. As shown in Fig. 3g, we quantified the computational time and corresponding emissions (expressed in grams equivalent per 48-cores node, g EqCO₂/48 cores) for each step involved in determining the GaP/Si interface energy. Single-point calculations on optimized structures were performed on 48 cores (one full node) of the Skylake partition at the Très Grand Centre de Calcul du CEA (TGCC) high-performance computing facility. The calculations underscore substantial differences in computational time and cost between reconstructed and H* passivated surfaces in GaP/Si interface energy evaluations. Notably, the H* passivated surface approach reduces simulation time by 25%, completing in just 0.9 hours compared to 1.2 hours for the reconstructed surface method, underscoring the processing efficiency of our approach. It is also worth noting that the single-point calculations performed here represent only a small fraction of the computational resources required for full relaxation calculations. Our analysis of greenhouse gas emissions further underscores the environmental benefits of our proposed method. As shown in Fig. 3g, the H* passivation approach yields emissions of only 7.5g EqCO₂ per 48 cores, in contrast to 15.5g EqCO₂ per 48 cores for the reconstructed surface method. This notable reduction comes from the smaller system size, reduced number of atoms, and lower charge requirements inherent to the H* passivation strategy.

Discussion

We introduced above a generalized, and computationally efficient methodology for determining absolute interface energies in heterostructures using density functional theory. Our approach systematically addresses and mitigates common sources of error, including uncertainties from guessed reconstructions, finite-size effects, convergence issues, and dipole artifacts. We demonstrated the robustness and versatility of the approach by applying it to both quasi-lattice-matched (GaP/Si) and lattice-mismatched (GaAs/Si) heterostructures. Despite the use of high k-point calculations, the fictitious H* passivation method not only

enhances computational efficiency but also significantly reduces resources consumption. Notably, it lowers greenhouse gas emissions by 50% compared to the surface reconstruction method, highlighting its potential for a more sustainable computational approach. This standardized approach can streamline heterointerface calculations by enabling the determination of absolute interface energy values and the investigation of fundamental principles governing diverse heterointerface configurations through *ab initio* approaches applicable to all material heterostructures (e.g. III-V, II-VI, IV semiconductors, oxides, perovskites, metals and semi-metals, 2D materials), including plastically relaxed systems. It provides an efficient framework and serves as a valuable tool for optimizing high-quality, cost-effective, and multifunctional devices across a broad range of applications, particularly in next-generation photonics, nanoelectronics, quantum technologies, energy conversion, and other emerging fields where precise interface control is essential.

Methods

Computational details:

All DFT calculations^{44,45} were performed using the SIESTA code⁵¹⁻⁵³, employing a basis set of finite-range numerical pseudo-atomic orbitals for the valence wave functions. The exchange-correlation effects were treated within the Generalized Gradient Approximation (GGA) functional in the Perdew-Burke-Ernzerhof (PBE) form⁶⁴. Core-valence interactions were described by Troullier-Martins (TM) norm-conserving pseudopotentials⁶⁵. Brillouin zone integrations were performed using a 4x2x1 and 6x6x1 Monkhorst-Pack k-point grid for surface reconstructed and H* passivated interfaces studies, respectively⁶⁶. For the strained GaAs/Si heterostructures, a real-space mesh cutoff of 300 Ry was employed, while a cutoff 150 Ry was used for the quasi-lattice-matched GaP/Si studies. To prevent interactions between periodic images, a vacuum region of approximately 400 Å was introduced along the vertical (z) direction of the substrate. Pseudopotentials for the fictitious Hydrogen-like (H*) atoms were generated using the ATOM code within the SIESTA package.

GaAs: Heat of formation energy

In a materials system, the chemical potential must satisfy specific thermodynamic constraints. The maximum values of the chemical potentials of arsenic μ_{As} and gallium μ_{Ga} are achieved when each element exists in its own pure bulk phase, leading to the conditions:

$$\mu_{As} < \mu_{As}^{As-bulk} \text{ and } \mu_{Ga} < \mu_{Ga}^{Ga-bulk}.$$

Furthermore, under thermodynamic equilibrium, the chemical potentials must satisfy the stability condition of the GaAs bulk phase: $\mu_{Ga} + \mu_{As} = \mu_{GaAs}^{GaAs-bulk}$. These constraints ensure that the GaAs material remains stable without decomposition into its elemental constituents. Thus,

$$\mu_{GaAs}^{GaAs-bulk} = \mu_{Ga}^{Ga-bulk} + \mu_{As}^{As-bulk} + \Delta H_f(GaAs) \quad (3)$$

Where $\Delta H_f(GaAs)$ denotes the heat of formation of GaAs material. In this work, $\Delta H_f(GaAs)$ is calculated to be -0.70 eV, which is in good agreement with the experimentally reported value -0.74 eV⁵⁶. This energy defines the thermodynamic stability window between Ga-rich and As-rich growth conditions, as illustrated in Fig. 2b.

The GaAs/Si interface energy is evaluated as a function of the variation in the arsenic chemical potential, defined as $\Delta\mu_{As} = \mu_{As} - \mu_{As}^{As-bulk}$. The thermodynamic limits for $\Delta\mu_{As}$ are given by:

$$\Delta H_f(GaAs) < \Delta\mu_{As} < 0 \quad (4)$$

when $\Delta\mu_{As}$ equals the heat of formation $\Delta H_f(GaAs)$, the system reaches the Ga-rich extreme limit, favoring the formation of bulk Ga. In contrast, when $\Delta\mu_{As}$ equals 0, the As-rich limit is achieved, leading to the preferential formation of bulk As.

Absolute interface energy using reconstructed surfaces

This approach enables the determination of all possible interface energies, independent of both the crystal orientation and the atomic structure of the interface. It also requires a detailed understanding of the free surface reconstructions and their corresponding energies. However, it involves heavy DFT calculations and substantial computational time. We define the absolute interface energy as $I_{Y_{Bottom}}^{Top}$, where I denote the studied interface. Top and

Bottom refer to the specific surfaces of the slab associated with the two materials under consideration. The absolute interface energy is defined as:

$$I_{\gamma_{\text{Bottom}}^{\text{Top}}} = \frac{E_{\text{slab}}^{\text{int}} - \sum_i (N_i \mu_i^{\text{i-bulk}}) - \sum_{S=\text{Top,Bottom}} (A \gamma_{\text{surf}}^S)}{A} \quad (5)$$

where $E_{\text{slab}}^{\text{int}}$ is the total energy of the slab, $\mu_i^{\text{i-bulk}}$ denote the chemical potentials of atom i in its bulk phase, N_i is the number of atom i , γ_{surf}^S represents the surface energies of the top or the bottom surfaces, and A is the in-plane surface area of the slab. Interestingly, Eqn. (5) highlights the explicit dependence of the interface energy on the chemical potentials of the constituent elements and the specific surface energies selected.

From the equation above, we can derive the relationship for the absolute interface energy of GaAs/Si, $I_{\gamma_{\text{Si}}^{\text{GaAs}}}$, where the GaAs(001) β 2(2x4) surface is on top of the slab at the GaAs part and the reconstructed Si(001)c(4x2) surface is at the bottom of the slab at the Si part.

$$I_{\gamma_{\text{Si}}^{\text{GaAs}}} = \frac{E_{\text{slab}}^{\text{GaAs/Si}} - N_{\text{GaAs}} \mu_{\text{GaAs}}^{\text{GaAs-bulk}} - (N_{\text{Ga}} - N_{\text{As}}) \mu_{\text{As}} - N_{\text{Si}} \mu_{\text{Si}}^{\text{Si-bulk}} - A \gamma_{\text{surf}}^{\text{GaAs}} - A \gamma_{\text{surf}}^{\text{Si}}}{A} \quad (6)$$

where $E_{\text{slab}}^{\text{GaAs/Si}}$ is the total energy of the slab, N_{Ga} and N_{As} represent the number of Ga and As atoms in the slab, $\mu_{\text{GaAs}}^{\text{GaAs-bulk}}$ and μ_{As} are the chemical potentials of the GaAs bulk and As species, and A is the surface area. $\mu_{\text{Si}}^{\text{Si-bulk}}$ is the chemical potential of silicon bulk, N_{Si} is the number of Silicon atoms, and $\gamma_{\text{surf}}^{\text{GaAs}}$ and $\gamma_{\text{surf}}^{\text{Si}}$ are the specific surface energies per unit area for the top and bottom surfaces of GaAs and Si, respectively.

Data availability

All data needed to evaluate the conclusions in the paper are present in the paper and/or the Supplementary Information. The other data that supports the findings of this study are available from the corresponding author upon request.

References

1. Kroemer, H. Nobel Lecture: Quasielectric fields and band offsets: teaching electrons new tricks. *Rev. Mod. Phys.* **73**, 783–793 (2001).
2. Kroemer, H. Heterostructure devices: A device physicist looks at interfaces. *Surface Science* **132**, 543–576 (1983).
3. O’Sullivan, M. *et al.* Interface control by chemical and dimensional matching in an oxide heterostructure. *Nature Chem* **8**, 347–353 (2016).
4. Pashley, M. D. Electron counting model and its application to island structures on molecular-beam epitaxy grown GaAs(001) and ZnSe(001). *Phys. Rev. B* **40**, 10481–10487 (1989).
5. Wang, L. G., Kratzer, P., Scheffler, M. & Moll, N. Formation and Stability of Self-Assembled Coherent Islands in Highly Mismatched Heteroepitaxy. *Phys. Rev. Lett.* **82**, 4042–4045 (1999).
6. Trampert, A. Heteroepitaxy of dissimilar materials: effect of interface structure on strain and defect formation. *Physica E: Low-dimensional Systems and Nanostructures* **13**, 1119–1125 (2002).
7. Supplie, O. *et al.* Atomic scale analysis of the GaP/Si(100) heterointerface by *in situ* reflection anisotropy spectroscopy and *ab initio* density functional theory. *Phys. Rev. B* **90**, 235301 (2014).
8. Borys, N. J., Walter, M. J., Huang, J., Talapin, D. V. & Lupton, J. M. The Role of Particle Morphology in Interfacial Energy Transfer in CdSe/CdS Heterostructure Nanocrystals. *Science* **330**, 1371–1374 (2010).
9. Mannhart, J. & Schlom, D. G. Oxide Interfaces—An Opportunity for Electronics. *Science* **327**, 1607–1611 (2010).
10. Van De Walle, C. G. & Martin, R. M. Theoretical study of band offsets at semiconductor interfaces. *Phys. Rev. B* **35**, 8154–8165 (1987).
11. Van De Walle, C. G. & Martin, R. M. Theoretical calculations of heterojunction discontinuities in the Si/Ge system. *Phys. Rev. B* **34**, 5621–5634 (1986).
12. Chen, L. *et al.* Strong Electron–Phonon Interaction in 2D Vertical Homovalent III–V Singularities. *ACS Nano* **14**, 13127–13136 (2020).

13. Romanyuk, O., Hannappel, T. & Grosse, F. Atomic and electronic structure of GaP/Si(111), GaP/Si(110), and GaP/Si(113) interfaces and superlattices studied by density functional theory. *Phys. Rev. B* **88**, 115312 (2013).
14. Romanyuk, O., Supplie, O., Susi, T., May, M. M. & Hannappel, T. *Ab initio* density functional theory study on the atomic and electronic structure of GaP/Si(001) heterointerfaces. *Phys. Rev. B* **94**, 155309 (2016).
15. Chen, W. *et al.* Enhanced solar hydrogen production via reconfigured semi-polar facet/cocatalyst heterointerfaces in GaN/Si photocathodes. *Nat Commun* **16**, 879 (2025).
16. George, B. M. *et al.* Atomic Structure of Interface States in Silicon Heterojunction Solar Cells. *Phys. Rev. Lett.* **110**, 136803 (2013).
17. Bushick, K., Chae, S., Deng, Z., Heron, J. T. & Kioupakis, E. Boron arsenide heterostructures: lattice-matched heterointerfaces and strain effects on band alignments and mobility. *npj Comput Mater* **6**, 3 (2020).
18. Gumbsch, P. & Daw, M. S. Interface stresses and their effects on the elastic moduli of metallic multilayers. *Phys. Rev. B* **44**, 3934–3938 (1991).
19. Hybertsen, M. S. Role of interface strain in a lattice-matched heterostructure. *Phys. Rev. Lett.* **64**, 555–558 (1990).
20. Wang, Y. *et al.* Mechanism of formation of the misfit dislocations at the cubic materials interfaces. *Applied Physics Letters* **100**, 262110 (2012).
21. Kroemer, H. Polar-on-nonpolar epitaxy. *Journal of Crystal Growth* **81**, 193–204 (1987).
22. Lucci, I. *et al.* Universal description of III-V/Si epitaxial growth processes. *Phys. Rev. Materials* **2**, 060401 (2018).
23. Pallikkara Chandrasekharan, S., Lucci, I., Gupta, D., Cornet, C. & Pedesseau, L. Determination of III-V/Si absolute interface energies: Impact on wetting properties. *Phys. Rev. B* **108**, 075305 (2023).

24. Rio Calvo, M. *et al.* Crystal Phase Control during Epitaxial Hybridization of III-V Semiconductors with Silicon. *Adv Elect Materials* **8**, 2100777 (2022).
25. Chen, L. *et al.* Epitaxial III–V/Si Vertical Heterostructures with Hybrid 2D-Semimetal/Semiconductor Ambipolar and Photoactive Properties. *Advanced Science* **9**, 2101661 (2022).
26. Cornet, C. *et al.* Zinc-blende group III-V/group IV epitaxy: Importance of the miscut. *Phys. Rev. Materials* **4**, 053401 (2020).
27. Tsai, H. *et al.* High-efficiency two-dimensional Ruddlesden–Popper perovskite solar cells. *Nature* **536**, 312–316 (2016).
28. Blancon, J.-C. *et al.* Extremely efficient internal exciton dissociation through edge states in layered 2D perovskites. *Science* **355**, 1288–1292 (2017).
29. Lucci, I. *et al.* A Stress-Free and Textured GaP Template on Silicon for Solar Water Splitting. *Adv Funct Materials* **28**, 1801585 (2018).
30. Ben Aziza, Z. *et al.* van der Waals Epitaxy of GaSe/Graphene Heterostructure: Electronic and Interfacial Properties. *ACS Nano* **10**, 9679–9686 (2016).
31. Hill, I. G. & Kahn, A. Energy level alignment at interfaces of organic semiconductor heterostructures. *Journal of Applied Physics* **84**, 5583–5586 (1998).
32. Calvin, J. J., Brewer, A. S., Crook, M. F., Kaufman, T. M. & Alivisatos, A. P. Observation of negative surface and interface energies of quantum dots. *Proc. Natl. Acad. Sci. U.S.A.* **121**, e2307633121 (2024).
33. Ponchet, A., Patriarche, G., Rodriguez, J. B., Cerutti, L. & Tournié, E. Interface energy analysis of III–V islands on Si (001) in the Volmer-Weber growth mode. *Applied Physics Letters* **113**, 191601 (2018).
34. Welch, E. & Scolfaro, L. Hybrid density functional theory study on zinc blende GaN and diamond surfaces and interfaces: Effects of size, hydrogen passivation, and dipole corrections. *Computational Condensed Matter* **30**, e00653 (2022).

35. Butler, K. T., Sai Gautam, G. & Canepa, P. Designing interfaces in energy materials applications with first-principles calculations. *npj Comput Mater* **5**, 19 (2019).
36. Beyer, A. *et al.* Pyramidal Structure Formation at the Interface between III/V Semiconductors and Silicon. *Chem. Mater.* **28**, 3265–3275 (2016).
37. Sun, L., Marques, M. A. L. & Botti, S. Direct insight into the structure-property relation of interfaces from constrained crystal structure prediction. *Nat Commun* **12**, 811 (2021).
38. Di Liberto, G., Morales-García, Á. & Bromley, S. T. An unconstrained approach to systematic structural and energetic screening of materials interfaces. *Nat Commun* **13**, 6236 (2022).
39. Liu, W., Li, J. C., Zheng, W. T. & Jiang, Q. Ni Al (110) / Cr (110) interface: A density functional theory study. *Phys. Rev. B* **73**, 205421 (2006).
40. Dietze, E. M. & Plessow, P. N. Predicting the Strength of Metal–Support Interaction with Computational Descriptors for Adhesion Energies. *J. Phys. Chem. C* **123**, 20443–20450 (2019).
41. Li, Y.-F. First-Principles Prediction of the ZnO Morphology in the Perovskite Solar Cell. *J. Phys. Chem. C* **123**, 14164–14172 (2019).
42. Pallikkara Chandrasekharan, S., Gupta, D., Cornet, C. & Pedesseau, L. Inevitable Si surface passivation prior to III-V/Si epitaxy: Strong impact on wetting properties. *Phys. Rev. B* **109**, 045304 (2024).
43. Müller, P. & Kern, R. Equilibrium nano-shape changes induced by epitaxial stress (generalised Wulff–Kaisheff theorem). *Surface Science* **457**, 229–253 (2000).
44. Hohenberg, P. & Kohn, W. Inhomogeneous Electron Gas. *Phys. Rev.* **136**, B864–B871 (1964).
45. Kohn, W. & Sham, L. J. Self-Consistent Equations Including Exchange and Correlation Effects. *Phys. Rev.* **140**, A1133–A1138 (1965).
46. Huang, X., Lindgren, E. & Chelikowsky, J. R. Surface passivation method for semiconductor nanostructures. *Phys. Rev. B* **71**, 165328 (2005).
47. Zhang, Y. *et al.* Pseudo-Hydrogen Passivation: A Novel Way to Calculate Absolute Surface Energy of Zinc Blende (111)/(111) Surface. *Sci Rep* **6**, 20055 (2016).

48. Jardine, M. J. A. *et al.* First-Principles Assessment of CdTe as a Tunnel Barrier at the α -Sn/InSb Interface. *ACS Appl. Mater. Interfaces* **15**, 16288–16298 (2023).
49. Jardine, M. J. A. *et al.* First-Principles Assessment of ZnTe and CdSe as Prospective Tunnel Barriers at the InAs/Al Interface. *ACS Appl. Mater. Interfaces* **17**, 5462–5474 (2025).
50. Tuoc, V. N., Huan, T. D. & Lien, L. T. H. Modeling study on the properties of GaN/AlN core/shell nanowires by surface effect suppression. *Physica Status Solidi (b)* **249**, 1241–1249 (2012).
51. Artacho, E., Sanchez-Portal, D., Ordejon, P., Garcia, A. & Soler, J. M. Linear-scaling ab-initio calculations for large and complex systems. *phys. stat. sol. (b)* **215**, 809–817 (1999).
52. Soler, J. M. *et al.* The SIESTA method for *ab initio* order- *N* materials simulation. *J. Phys.: Condens. Matter* **14**, 2745–2779 (2002).
53. Artacho, E. *et al.* The SIESTA method; developments and applicability. *J. Phys.: Condens. Matter* **20**, 064208 (2008).
54. Makov, G. & Payne, M. C. Periodic boundary conditions in *ab initio* calculations. *Phys. Rev. B* **51**, 4014–4022 (1995).
55. Bennett, D., Pizzochero, M., Junquera, J. & Kaxiras, E. Accurate and efficient localized basis sets for two-dimensional materials. *Phys. Rev. B* **111**, 125123 (2025).
56. Ohtake, A., Kocán, P., Seino, K., Schmidt, W. G. & Koguchi, N. Ga-Rich Limit of Surface Reconstructions on GaAs(001): Atomic Structure of the (4 × 6) Phase. *Phys. Rev. Lett.* **93**, 266101 (2004).
57. Kroemer, H., Liu, T.-Y. & Petroff, P. M. GaAs on Si and related systems: Problems and prospects. *Journal of Crystal Growth* **95**, 96–102 (1989).
58. Pohl, U. W. *Epitaxy of Semiconductors: Physics and Fabrication of Heterostructures*. (Springer International Publishing, Cham, 2020). doi:10.1007/978-3-030-43869-2.
59. Boettger, J. C. Nonconvergence of surface energies obtained from thin-film calculations. *Phys. Rev. B* **49**, 16798–16800 (1994).

60. Scholz, D. & Stirner, T. Convergence of surface energy calculations for various methods: (0 0 1) hematite as benchmark. *J. Phys.: Condens. Matter* **31**, 195901 (2019).
61. Kezerashvili, R. Ya. & Kezerashvili, V. Ya. Charge-dipole and dipole-dipole interactions in two-dimensional materials. *Phys. Rev. B* **105**, 205416 (2022).
62. Kusunose, H. & Hayami, S. Generalization of microscopic multipoles and cross-correlated phenomena by their orderings. *J. Phys.: Condens. Matter* **34**, 464002 (2022).
63. Zheng, H., Zhai, D., Xiao, C. & Yao, W. Interlayer Electric Multipoles Induced by In-Plane Field from Quantum Geometric Origins. *Nano Lett.* **24**, 8017–8023 (2024).
64. Perdew, J. P., Burke, K. & Ernzerhof, M. Generalized Gradient Approximation Made Simple. *Phys. Rev. Lett.* **77**, 3865–3868 (1996).
65. Troullier, N. & Martins, J. L. Efficient pseudopotentials for plane-wave calculations. *Phys. Rev. B* **43**, 1993–2006 (1991).
66. Monkhorst, H. J. & Pack, J. D. Special points for Brillouin-zone integrations. *Phys. Rev. B* **13**, 5188–5192 (1976).

Acknowledgements

This research was supported by the French National Research NUAGES Project (Grant no. ANR-21-CE24-0006). DFT calculations were performed at FOTON Institute, and the work was granted access to the HPC resources of TGCC/CINES under the allocation A0140911434, A0160911434, and A0180911434 made by GENCI.

Author contributions

S.P.C. conducted the investigation, carried out formal analysis, curated the data, and prepared the original draft. S.A. contributed to data analysis and manuscript review and editing. C.C. and L.P. conceived the study, performed methodology development, supervised the project, validated the results, contributed to data analysis, manuscript review and editing,

and contributed to project administration and conceptualization. C.C. acquired funding, and L.P. was responsible for resource management.

Competing interest

The authors declare no competing interests.

Additional information

Supplementary information The online version contains supplementary material available at

Correspondence and requests for materials should be addressed to Charles Cornet and Laurent Pedesseau.